Influence of the Pyrolysis Conditions on the Nature of Lithium Inserted in Hard Carbons

S. Gautier,[†] F. Leroux,[†] E. Frackowiak,[‡] A. M. Faugère,[†] J.-N. Rouzaud,[†] and F. Béguin*,[†]

Centre de Recherche sur la Matière Divisée, CNRS-Université, 1B, rue de la Férollerie, 45071 Orléans Cedex 2, France, and Institute of Chemistry and Technical Electrochemistry, Poznan University of Technology, ul. Piotrowo 3, 60-965 Poznan, Poland

Received: November 9, 2000; In Final Form: February 28, 2001

The influence of different heating processes of a fibrous cellulose precursor together with the application of anisotropic mechanical stretching has been studied for the Li storage in the obtained hard carbons. A reversible capacity up to 470 mAh/g has been reached and its origin has been associated with a large plateau at low potential vs Li. The ^{7}Li NMR spectrum recorded on the fully lithiated sample at room temperature presents a peak at 66 ppm. At lower temperature down to 230 K, this contribution is split into a temperature-independent peak centered at 18 ppm and an ill-defined paramagnetic shift. On the basis of the spin−lattice relaxation times, it is shown that the temperature-independent Li sites exhibit a small deviation to the Korringa type behavior at low temperature, that is associated with a distance between Li sites of the same order as for Li−Li in the metallic state. The paramagnetic NMR contribution has been related to the lithium ions inserted below 100 mV vs Li within the hard carbon. The reversibility of the electrochemical process, and especially the polarization between insertion and removal of the Li ions, is found to be related to their chemical nature, different if they are located in the nanopores or between the graphitic type layers. The data for inserted lithium in these samples clearly shows that extended delocalization of conduction electrons is not occurring.

Introduction

Intensive research has been devoted to carbon materials as negative electrodes in lithium-ion batteries.[1] It is well-known that a carbonaceous material to be considered as a relevant candidate in that field must have a large reversible capacity for lithium insertion/extraction, a small irreversible component, and a hysteresis as small as possible. Numerous carbons, such as graphite, petroleum cokes, pitch cokes, and mesocarbon microbeads, were studied for this electrochemical application.[2−4] In the past few years, many works were focused to understand the mechanism of lithium storage in order to simulate the intercalation and/or insertion process, and after to tune the carbon materials synthesis for getting better performance. The lithium intercalation mechanism into graphite is well established and is often used as a model for the other carbon materials. One lithium ion per six carbons, nominal composition of LiC_6, can be reached in standard conditions. This corresponds to a theoretical reversible specific capacity of 372 mAh/g. In this model, Li ions present in the interlamellar space are located at the center of the carbon hexagons, leading to a $\sqrt{3} \times \sqrt{3}$, 30° commensurate surstructure.[5]

Higher capacities have been obtained with hard carbons prepared by pyrolysis of different organic precursors such as saccharose at around 1000 °C.[6] However, some problems arise from the use of hard carbons as anode materials. Large irreversible capacities accompanied by a significant hysteresis are often observed. In contrast to the well-ordered layers stacking of graphite, low-temperature (about 1000 °C) hard carbons are constituted of short graphene layers (about 1 nm in diameter), sometimes single, but usually piled up, more or less in parallel, by 2 or 3 forming nanometric basic structural units (BSU).[7,8] The BSU are assumed to be connected to each other by sp^3 carbon atoms, and by heteroatoms such as oxygen, grafted on the boundaries of the graphene layers. The resulting cross-linking of the BSU is responsible for their random distribution and for the microporous microtexture of such hard carbons. Moreover, numerous carbon−hydrogen bonds remain present at the edge of the graphene layers. This accounts for the difficulty to simulate Li insertion into these poorly organized carbons. Numerous mechanisms have been proposed,[9−13] using the comparison to graphite. It was proposed by some authors that Li ions insertion into hard carbon proceeds via the filling of nanopores,[10] creating then some cluster-type lithium. Sometimes the insertion is presented as an adsorption process onto the graphene sheets.[11−13] But generally, as the hard carbons presented in the literature are different from each other, by their chemical composition and their microtexture, it is somehow difficult to disentangle the insertion process as a simple function of the Li ions density.

In this paper, a fibrous cellulose precursor has been submitted to different heating processes and the effect of mechanical stretching has been studied on lithium storage. The electrochemical characteristics are discussed in term of the microtexture, i.e., the spatial distribution of the BSU, and of the chemical composition. To unravel the nature of the inserted lithium ions and especially those inserted at low potential ($V <$ 100 mV vs Li), solid state ^{7}Li NMR temperature dependence has been performed for the samples containing different amounts of lithium. The NMR shift positions and the spin−lattice relaxation times were studied as a function of the cutoff potential (i.e., degree of Li storage), and analyzed in term of the Li ionicity/covalency within the hard carbon. The influence of mechanical stretching on the nature of lithium stored in the microtexture of hard carbon is addressed for the first time.

* Author to whom correspondence should be addressed at CRMD-CNRS, 1B, rue de la Férollerie, 45071 Orléans cedex 2, France. Phone: 33-2 38 25 53 75. Fax: 33-2 38 63 37 96. E-mail: beguin@cnrs-orleans.fr.

[†] CNRS-Université.

[‡] Poznan University of Technology.

10.1021/jp000892p CCC: $20.00
Published on Web 05/18/2001

Experimental Section

Carbons. An oxygen-rich cellulose precursor was used to prepare hard carbon fibers. The materials were carbonized under nitrogen atmosphere in semi-industrial furnaces. The first sample (sample 1) was heat-treated until 450 °C with a slight heating rate for two weeks in a batch oven and then at 1000 °C for one minute. The second sample (sample 2) was heat-treated 7 min at 450 °C and one minute at 1000 °C. For the third sample (sample 3), stretching was applied during the pyrolysis performed in the same conditions as for sample 2 in order to compensate for shrinkage due to evolution of volatile compounds.

Electrochemical Testing. A two-electrode cell was used with a lithium disk as counter and reference electrode and the fibrous carbon without binder as the working electrode. The carbon electrodes were dried at 140 °C for 12 h under vacuum. The electrolyte used was 1M $LiPF_6$ dissolved in a 1:1 mixture of ethylene carbonate (EC) and diethyl carbonate (DEC) (battery grade solvents, Merck). A microporous separator (Celgard 2500, Hoechst Celanese) was sandwiched between the carbon material and the lithium disk. The cell was assembled in a screwed Swagelok construction in a glovebox under argon atmosphere. Discharge (lithium insertion) and charge (lithium extraction) curves were obtained with a Mac Pile generator (Biologic, France). The cells were investigated from 3 V to −0.020 V vs Li/Li^+ with a constant current density of 20 mA/g of carbon material. The discharge cutoff voltage of −20mV was selected in order to partly take into account lithium metal passivation and its associated overpotential effect. For complementary electrochemical results, the cells were duplicated and examined under potentiostatic conditions with a voltage step of 10 mV per 0.2 h. Concerning the galvanostatic intermittent titration technique (GITT), current pulses of 15 mA/g were applied for 2.4 h, that corresponds to the insertion of 0.05 Li per six atoms of carbon (18.6 mAh/g) for each pulse. The evolution of the equilibrium potential between the pulses is measured by allowing the system to relax at open circuit during 24 h.

TEM. The microtexture characterization of the hard carbon fibers was realized by high-resolution transmission electron microscopy (Philips CM20 working at 200 kV). The sample was ground in anhydrous alcohol, then sonicated and a droplet was put on a copper grid covered by a holey carbon film. The profile of the carbon layers was imaged using the 002 lattice fringes mode.[7]

^{7}Li NMR Analysis. The carbon electrodes were examined by solid state ^{7}Li NMR using a Bruker 360 spectrometer (^{7}Li resonance frequency of 139.9 MHz). Each sample was allowed to stabilize 1 day after reaching the chosen potential. The electrode materials were dried overnight in the glovebox and sealed in a NMR probe. To avoid any degradation, excess of free salt from the electrolyte has not been eliminated by washing, therefore it could be used as an "internal" standard for the line position of ionic lithium. The ex-situ experiments, using a $\pi/2-\tau$ acquisition sequence, were performed in a static mode for the low-temperature conditions ($T<$ 293 K). Magic-angle spinning (MAS) spectra were recorded for the room-temperature part ($T = 293$ K) at a spinning rate of 8 kHz. The external standard used for the calibration was an aqueous solution of LiCl. For each spectrum, a recycle delay of at least $5T_1$ was employed to allow the lithium magnetization to return to Boltzmann equilibrium. The variations of the spin−lattice relaxation times, T_1, were studied versus temperature, using an inversion recovery sequence ($\pi-\tau-\pi/2$ acquisition).

TABLE 1: Elemental Composition of the Hard Carbon Samples (wt %); An Atomic Composition Is Given To Summarize These Data together with the Carbon/Oxygen Atomic Ratio

sample	C (%)	H (%)	O (%)	composition	C/O
1	93.48	0.56	1.41	$C_{0.92}H_{0.07}O_{0.01}$	88.4
2	93.08	0.69	4.12	$C_{0.89}H_{0.08}O_{0.03}$	30.1
3	93.16	0.56	3.80	$C_{0.91}H_{0.06}O_{0.03}$	32.7

Results and Discussion

Characterization of the Carbon Samples. The elemental analyses (Table 1) show that a pretreatment at 450 °C, followed by a short heating at 1000 °C, is able to get release an important part of the heteroatoms, since the carbon content is about 93% for the 3 samples. In these conditions, it is known that the elimination of heteroatoms, especially oxygen, is not completed as emphasized with the C/O atomic ratio, giving rise to losely organized carbons. A rapid treatment at 450 °C followed by the 1000 °C-temperature process (samples 2 and 3) gives three times higher oxygen content than in sample 1. It is noteworthy that the main difference in sample 1 and sample 2 is the time of pyrolysis at 450 °C. The main difference between samples 2 and 3 is the anisotropic stretching applied during the pyrolysis for sample 3. It appears that these samples contain the same oxygen amount, the hydrogen content remaining also the same (Table 1). Raman spectroscopy was performed on samples 1 and 2. No noticeable difference was observed in their spectra, indicating that the sp^2 and sp^3 relative populations are almost identical.

Figure 1a shows a TEM image of sample 1. Single fringes could be imaged, especially at the thin border of the fragment. Some BSU composed of only two or three graphene layers are observed. The microtexture is typical for a disordered hard carbon heat-treated at 1000 °C.[7,8] The single layers and the BSU are strongly disoriented, as exemplified by the presence of a complete ring in the Fourier transform (FT) pattern relative to this image (inset Figure 1a). Such disorientation leads to a microporous carbon as confirmed by the type I isotherm of nitrogen adsorption at 77 K. For the hard carbon fibers pyrolyzed under stretching (sample 3), there is a tendency to a parallel orientation of longer layers (Figure 1b). This is confirmed by the presence of two arcs in the FT pattern (inset Figure 1b). This orientation is limited to only few nanometers if stretching is applied during the pyrolysis of cellulose fibers, whereas soft carbons are characterized by a parallel orientation of the BSU within domains of micrometric size. It explains why sample 3 could not be transformed into graphite after a heat treatment at 2800 °C, contrary to a soft carbon.

Electrochemistry. Figure 2 shows the voltage profile curves for the hard carbons prepared according to three different conditions. The samples exhibit the same main feature, as expected for carbonaceous materials, i.e., a low average Li extraction potential associated with a relative good reversibility. Only the first two discharge and charge characteristics are presented in Figure 2. The difference between the first discharge and the first charge is taken as the irreversible capacity component, Q_{irr}. The reversible capacity, Q_{rev}, is defined as the first charge capacity. A shorter heating at 450 °C coupled with stretching applied during this process seems to be an advantage to obtain a larger reversible capacity. Sample 3 exhibits a reversible capacity of ca. 470 mAh/g (Table 2), which is larger than that found for graphite (372 mAh/g). In the same conditions of constant current density, sample 1 gives a reversible capacity of only ca. 240 mAh/g. The insertion of Li ions is associated with a relatively large irreversible loss during the first cycle, as

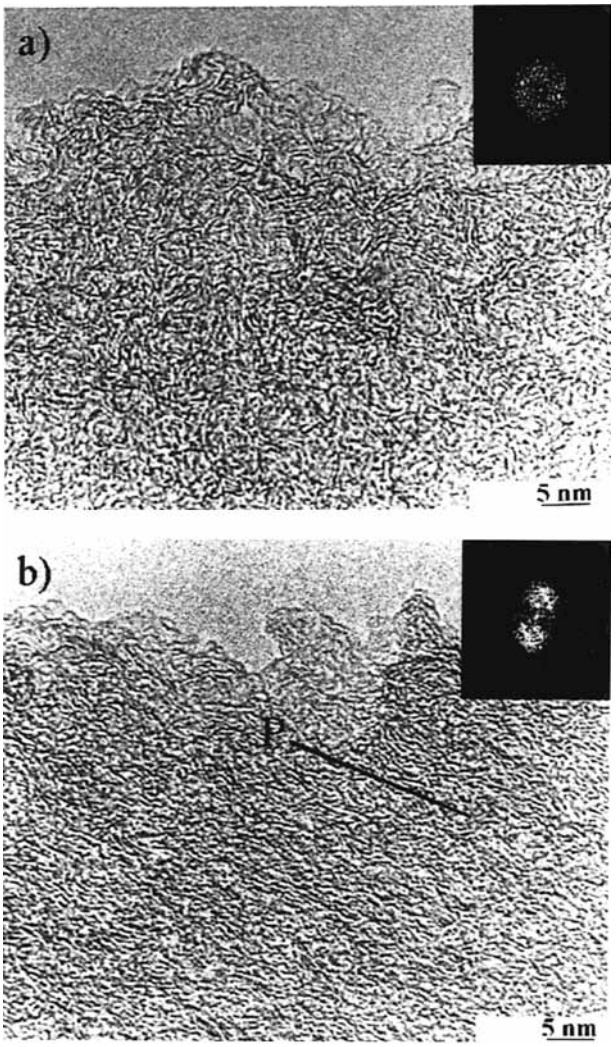

Figure 1. TEM images (002 lattice fringes) of (a) sample 1, and (b) sample 3. Line P indicates the trace of the plane of preferential orientation in (b). The insets are the Fourier transform patterns relative to the images.

large as 28 and 37% of the total first discharge capacity for samples 3 and 1, respectively. An optimized process is required to decrease the irreversible part of the first discharge capacity.

Apart of galvanostatic charge/discharge curves, potentiodynamic experiments were performed to elucidate the lithium insertion in details (insets in Figure 2). An irreversible cathodic current peak centered at 1 V (corresponding to the ill-defined plateau on the galvanostatic curves) is observed in the first discharge for all the samples. This irreversible contribution is characteristic for the decomposition of electrolyte, i.e., the formation of a solid/electrolyte interphase (SEI). The potential of the SEI formation is quite high for all the electrode materials (~1 V vs Li). This may be explained by the insertion of solvated Li cations in the large interlayer intervals of the hard carbon prior to electrolyte decomposition. Concerning the Li storage, the difference between the samples appears more clearly on the potentiodynamic curves. For sample 3, an anodic peak at 200 mV is clearly observed whereas no such contribution exists for sample 1. This suggests that the lithium ions deinsertion proceeds via an almost continuous mechanism for sample 1, whereas two steps are needed for sample 3. This Li deinsertion profile is related to the Li ions stored in the low voltage portion (V=100 mV), and noted as Q_a in Table 2. A large part of the reversible capacity of sample 3 is due to Q_a, whereas it is much less for the two other samples.

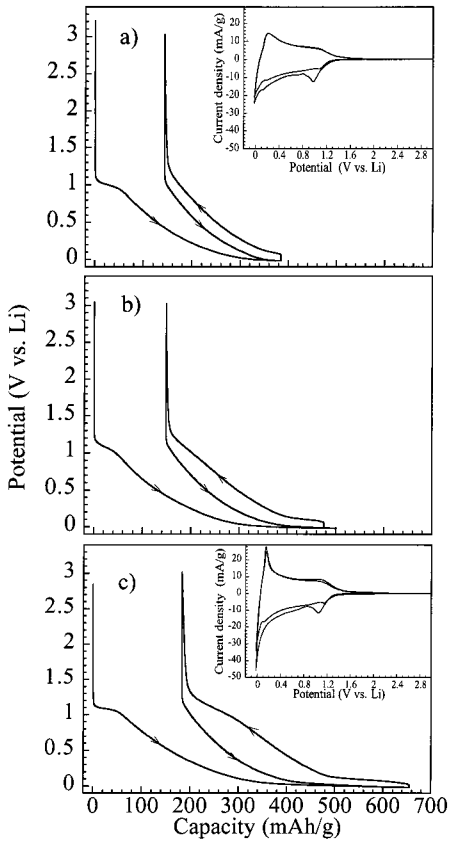

Figure 2. Voltage profile curves within the 3 V to −20 mV vs Li potential domain for (a) sample 1, (b) sample 2, and (c) sample 3. A current density of 20 mA/g was used. The insets show the potentiostatic curves for the respective samples; a voltage step of 10 mV per 0.2 h was used.

TABLE 2: Electrochemical Characteristics for Constant Current (20 mA/g) Experiments in the Potential Range from 3 V to −0.020 V vs Li[a]

sample	Q_{rev} (mAh/g)	Q_{irr} (mAh/g and %)	$n_{5/1}$ (%)	Q_a (%)
1	241	143 (37)	97	58
2	327	148 (31)	87	64
3	472	183 (28)	78	78

[a] Q_{rev} is the reversible capacity corresponding to the first charge. Q_{irr} is the irreversible capacity with its percentage relatively to the first discharge capacity. $n_{5/1}$ is the charge capacity retention at the fifth charge compared to the first. Q_a is the part of capacity obtained below 100 mV during the second discharge compared to its total value

A closer examination reveals that a noticeable hysteresis is associated with the response of sample 3. On the other hand, a large discharge plateau is observed for this sample at low potential. The question is to know if these two electrochemical characteristics are connected. In fact the potential step close to 0 V appearing when reversing the current is varying with the origin of the sample (Figure 2), due to different electrical resistivity. This suggests that stopping the discharge at −0.020 V does not allow full lithium insertion in the carbon material. Therefore, a short circuit was imposed to the cell at the end of the first discharge in order to reach the maximum lithium storage capability of samples 1 and 3, and the subsequent charge was measured (Figure 3 − dashed line). For sample 1 (Figure 3a), the reversible capacity increases from ~240 to 410 mAh/g, the later value being close to the capacity obtained for sample 3. This is also accompanied by an increase of the low voltage plateau length, Q_a, and a noticeable increase of the polarization. The curve feature and capacity remain almost the same for

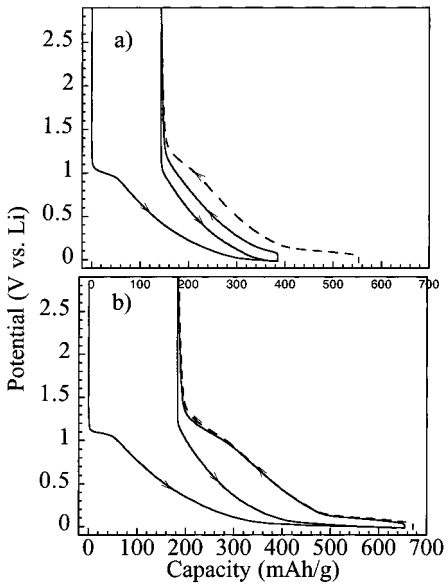

Figure 3. Short-circuit experiments on (a) sample 1, and (b) sample 3. The continuous line shows the voltage profile in the conditions of Figure 2, and the dashed line the charge when a short-circuit is applied during 24 h after the discharge at constant current.

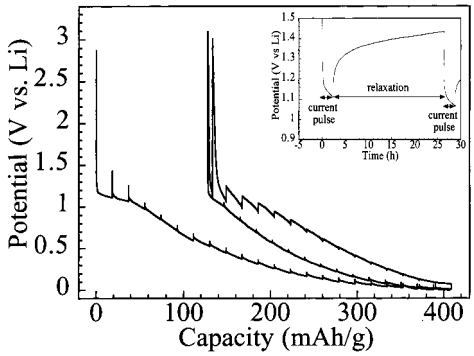

Figure 4. GITT experiment on sample 1. Each pulse under constant current corresponds to the insertion of 0.05 Li for 6 carbon atoms during 2.4 h. A 24 h time period was used as relaxation time between each pulse. The inset shows a current pulse during discharge and the subsequent relaxation period.

sample 3 (Figure 3b). This shows clearly that the polarization is inherent to the Li ions inserted in the low voltage region and not to the oxygen content as suggested by some authors.[14]

Different origins may explain this hysteresis. At first, to define if it is related to a kinetic or thermodynamic effect, a GITT experiment was carried out on sample 1 (Figure 4), to determine potentials at a state of "quasi" equilibrium. The cell is submitted alternatively to weak discharge or charge pulses and to open circuit periods (relaxation) as shown in the inset of Figure 4. A relatively high potential drop is observed at the beginning of the first discharge that is due to the formation of an electronically insulating solid/electrolyte interphase**,** which at this step of the process has a dominant contribution on the overall resistivity of the electrode. Proceeding with discharge, the ohmic drop becomes rapidly negligible reflecting the effect of lithium insertion with a charge transfer to the carbon matrix. During the first part of charge, from −0.020 V until ca. 0.8 V vs Li, the potential under current load is very close to equilibrium value due to the high conductivity of the doped electrode. Above 0.8 V vs Li, the potential drop between load and relaxation periods becomes higher and higher, especially at the end of lithium extraction, revealing the intrinsic resistive nature of the delithiated electrode material. ^{7}Li NMR results presented further in this paper show that this second part of the charge is related with the progressive elimination of metallic lithium clusters, without important charge transfer to carbon. Therefore resistivity of the electrode becomes more and more comparable to that of the pristine material covered by the passivating layer. Finally GITT shows that there is still a hysteresis even operating in conditions close to thermodynamic equilibrium (Figure 4). The structure and the microtexture of the hard carbon material are responsible for this contribution.

The sample 1 sustains a relatively good cyclability (Table 2), as exemplified by a charge capacity retention of 97% after the fifth cycle, whereas it is worse for the samples 2 and 3. In the latter, it is explained by the nature of the inserted Li ions, as it will be shown by the ^{7}Li NMR study. However, such a fade could be also related to the relatively high amount of oxygen present in samples 2 and 3.

Few questions arise from the electrochemical experiments. As Q_a represents a large part of the reversible capacity, it is important to know what is the nature of the related lithium species and why it is different from the other response. Another question would be to know how the polarization is connected to the Li ions inserted below 100 mV.

^{7}Li NMR Spectroscopy. Three main interactions govern the shape of ^{7}Li solid-state NMR spectra—the quadrupole, the dipole, and the chemical shift. The quadrupole interaction arises from an asymmetric charge distribution (^{7}Li spin of 3/2) creating a moment coupled to the local electric field. The quadrupolar coupling constant for ^{7}Li is small, giving rise generally only to the observation of the central line, corresponding to the transition $m = 1/2 \rightarrow -1/2$. This transition is observed on the lithiated hard carbons. A magic angle spinning (MAS) experiment was performed on the sample 1 at the end of the first discharge (−0.02 V) and on the sample 3 during the first charge and discharge at different values of the cutoff potential (Figure 5). MAS conditions reduce the line width of the NMR peak, when compared to the static mode condition, as exemplified with the decrease of half width from 7.1 kHz to 5.2 kHz for the signal at room temperature (Figure 5). Quadrupolar satellites are not present, whereas they were previously observed in the case of ordered Li phases such as in-plane surstructures into graphite.[15] It seems that the lithium ions are not organized in an ordered fashion or that the eventual Li islands are enough dispersed within the hard carbons. This is observed for all the values of potential cutoff, even for the highest degree of Li insertion for which some organization could be expected due to the dense packing of Li ions. Two cases must be taken into account in order to explain the absence of satellite transitions: (i) an exchange of the Li ions of a homogeneous nature, (ii) an inhomogeneous nature of site for static Li. Both effects give then rise to a spreading of the satellite transitions in the background of the spectrum.

At a first glance, the ^{7}Li NMR line shift increases as lithium insertion into carbon proceeds (Figure 5). It is commonly accepted that, due to the light nature of ^{7}Li nucleus, a value in the range from 0 to 6 ppm would correspond to a "true" chemical shift. For instance, the presence of Li salts (arising from the electrolyte) is demonstrated by a peak centered at ∼0 ppm. Coming from this range, the peak is shifted toward a downfield direction with the Li ions insertion, meaning that the average positive charge on all the lithium inserted within the hard carbon is decreasing with the increase of capacity (Table 3). A value of 66 ppm was observed for the sample 3 at the end of the first discharge, greater than that for graphite with $\delta = 42$ ppm in the case of LiC_6. Shifts up to 110 ppm were found

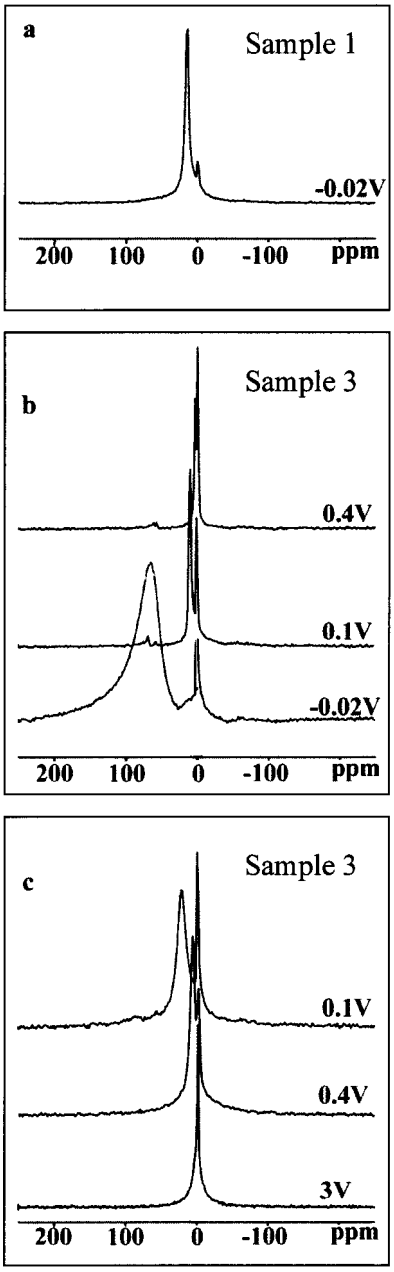

Figure 5. Room-temperature ^{7}Li NMR MAS spectra of (a) sample 1 at the end of the first discharge (−0.02 V), (b) sample 3 for different cutoff potentials (0.4, 0.1, and −0.02 V) in the first discharge, and (c) sample 3 for different cutoff potentials (0.1, 0.4 and 3 V) in the first charge. The spinning rate was 8 kHz.

TABLE 3: Evolution of the Li Shift with the Cut-off Potential in mV vs Li[a]

	sample 1	sample 3				
cut-off potential	−20 (D1)	400 (D1)	100 (D1)	−20 (D1)	100 (C1)	400 (C1)
δ (ppm)	15	3	10	66	22	8

[a] The shift of the line is given by the MAS ^{7}Li NMR experiments performed at 293 K. D1 and C1 indicate the nature of the electrochemical process, first discharge, and charge, respectively.

for lithiated hard carbons.[16−23] The discrepancy for the values of δ may come not only from the Li chemical bonding but also from the experimental conditions. Contrary to some observations on nongraphitizable carbons,[17] it is interesting to note that in our case the shift value is not equivalent for the same potential in both redox processes, δ being greater for the charge than for the discharge (Table 3). A different kind of lithium bonding could be the explanation for the polarization observed on the voltage profile curves. Some other authors have even reported that a shift of 45 ppm was still present at the end of the first cycle.[18] In our case, a shift of 0 ppm is observed, related to the electrolyte salt and the decomposition products such as Li_2CO_3 and Li_2O.

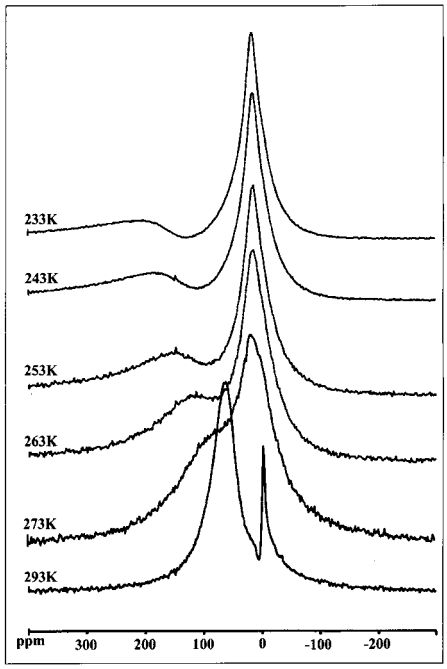

Figure 6. Temperature dependence of the static ^{7}Li NMR spectrum for sample 3 (after a discharge to −20 mV vs Li).

To precise the nature of the peak at 66 ppm, ^{7}Li NMR experiments have been performed at low temperature. It is noteworthy that the electrolyte diamagnetic signal is disappearing, due to the broadening by the freezing of the Li ion motion. The other peak is split into two contributions below 273 K—one peak at 18 ppm independent of temperature, which may correspond to a Knight shift component, and another peak shifted toward larger values with the decrease of temperature (Figure 6). The former is interpreted as a Fermi contact interaction term coming from the hyperfine interaction between the 2s state and the conduction electron (Pauli paramagnetism). With the temperature decrease, this splitting is associated with a large broadening of the paramagnetic peak, that is explained by the decrease of the exchange motion for the Li nuclei.[19,21−23] The exchange process, which is clearly evidenced in Figure 6, involves then the motion of lithium ions between sites, spatially or electronically different. The whole phenomenon is generally explained by a complex multisite exchange process.[24] Significantly, a temperature-independent position of the peak was observed either for the sample 1 at the end of the first discharge or for the sample 3 at 400 and 100 mV during the first discharge and at 400 mV during the first charge. This is showing that the splitting behavior is only relative to the Li inserted below 100 mV.

The population and half width associated with the different contributions were studied after full discharge (−20 mV) for the low temperature portion (Figures 7 (sample 1) and 8 (sample 3)). For a better understanding, the deconvolution of the line recorded at 263 K is also shown. For the sample 1, an inversion of population is observed between apparently a very diffusive Li ($\delta \sim 12$ ppm at room temperature, associated with a width at half-height, $\Delta\nu_{1/2}$, of 8 to 10 kHz) and a contribution at higher

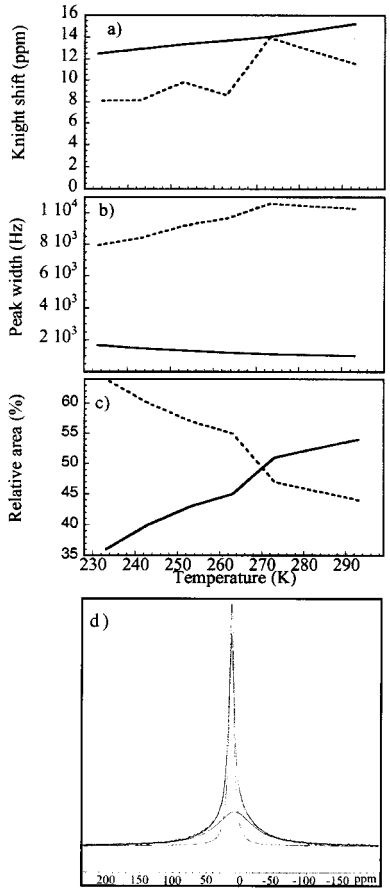

Figure 7. Temperature dependence of ^{7}Li NMR parameters of the line for sample 1 (end of discharge): (a) shift, (b) line width, (c) relative area, and (d) deconvolution of the static ^{7}Li NMR spectrum recorded at 263 K.

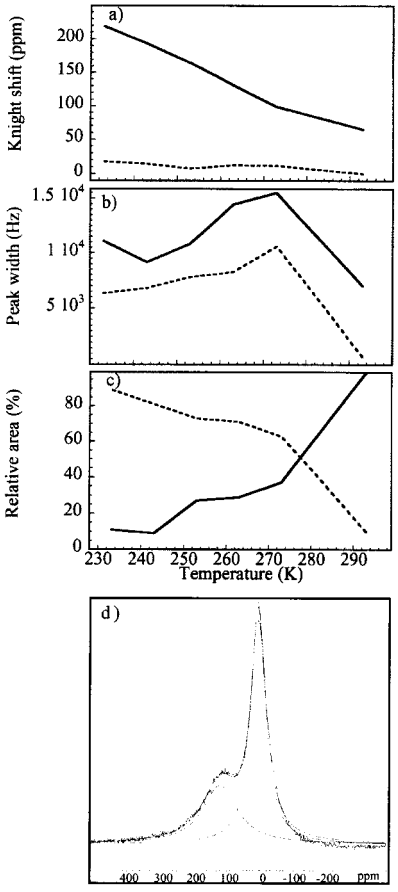

Figure 8. Temperature dependence of ^{7}Li NMR parameters of the line for sample 3 (end of discharge): (a) shift; (b) line width; (c) relative area, and (d) deconvolution of the static ^{7}Li NMR spectrum recorded at 263 K.

shift ($\Delta\nu_{1/2}$ of 1 to 2 kHz). One has to note that Li ions have typically a very short lifetime on the same site. This is the broadening effect mentioned before, and the line shape is then transformed by time averaging into a narrow Lorentzian with extended wings. As this is observed for all the temperature down to 230 K with a same width, the meaning of the extended wings needs to be modulated. Single pulse sequence is also known to introduce artificially a large baseline due to the loss of beginning of free induction decay.[24] For the sample 3, the relative area of the paramagnetic contribution is smaller when the temperature decreases. The half width variations of this component at low temperature are somewhat difficult to interpret, but its width value at 233 K (~12 kHz) is close to what is observed for Li metal (Figure 9b). The Knight shift of Li metal is observed as a much sharper contribution ($\delta = 262$ ppm) at room temperature (Figure 9a). By freezing the motion of the spin system, the dipolar structure is then accessible on the central line, and varies proportionally to μ/r^3, r being the lithium dipole−dipole distance. The central line is not affected by the first-order quadrupole interaction, only by the much smaller second-order quadrupole interaction. In dense matter the ^{7}Li NMR line width is generally governed by the local magnetic fields produced by the high magnetic moment of the first Li neighbors.[25] Since the proton content in the electrode material is in the order of 0.6 wt % (Table 1), we consider that the line broadening at low temperature is arising from a homonuclear Li−Li dipolar interaction. The comparison let us then conclude, from these dipolar structure considerations, that the distance between Li sites is close to the Li−Li distance in metallic lithium (3.04 Å

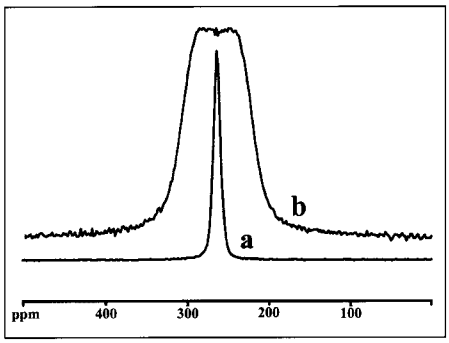

Figure 9. ^{7}Li NMR spectra of lithium metal at (a) room temperature, and (b) 233 K.

in the cc phase). For a comparison, the Li−Li distance in the dense graphitic phase, LiC_6, is of 4.3 Å.

It is commonly accepted that the nongraphitizable carbons possess "microcavities between the grains " as imaged by TEM (see Figure 1a). The paramagnetic shift on the spectra should be assigned to lithium ions trapped inside these cavities, clustering between each other and presenting a pseudometallic nature. This shift may be explained by some electronic overlapped orbitals, the lithium ions onto the surface of this pores being in contact to the carbon atoms. A size dependence of lithium cluster may be the issue for this phenomenon.

Further information is coming from the spin−lattice relaxation times, T_1, presented in an Arrhenius-law type in Figure 10a. With the applied low temperature, it is shown that T_1 increases, suggesting that the Li species are less and less mobile. No

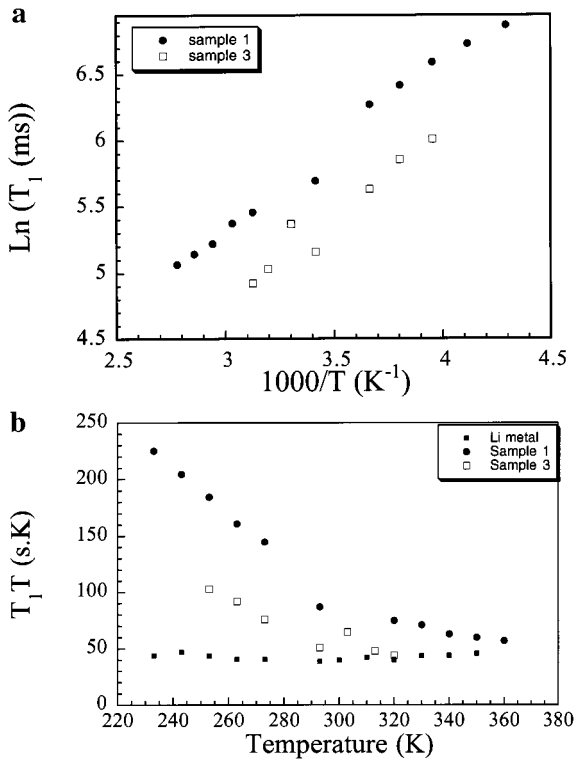

Figure 10. (a) Arrhenius presentation of the variation of the spin−lattice relaxation time, T_1, vs $1/T$ for samples 1 and 3 at −20 mV in the first discharge. (b) $(T_1 \times T)$ vs T (Korringa law fashion) for samples 1 and 3 at −20 mV. The data for lithium metal are shown for comparison.

pronounced minimum for T_1 was found, but rather the T_1 profiles exhibit a complicated feature, leaving no easy interpretation. A particular feature of ln T_1 vs $1/T$ was observed for sample 3 at full discharge (−20 mV). In Figure 10b, the relaxation times are given by a $(T_1 \times T)$vs T representation. Li metal obeys the relation $(T_1 \times T) =$ constant, which is the Korringa law. The value of the Knight shift is proportional to the electron density at a nucleus. The nature of Li in sample 3 at full discharge is thus not truly metallic (Figure 10b). The situation of Li sites at 18 ppm, as exemplified by sample 1, is between the case of an ionic nature and the case of the lithium metal. A density of state of 0.1 was found for Li in sample 3 according to its Knight shift [26] at room temperature (66 ppm), i.e., 10% of the 2s electron is located on the lithium nucleus, thus leading to an apparent valency of 0.9. In contrast, a density of state of 0.37 is obtained for the paramagnetic component at low temperature.

Conclusion

Varying pyrolysis conditions and depending on whether anisotropic stretching is applied or not during the pyrolysis of the polymeric precursor, the reversible capacity reaches either 470 mAh/g or 240 mAh/g. Anisotropic stretching applied during the heat treatment provokes a preferential local orientation of the graphene layers, and the better capacity for these materials is connected with a long potential plateau appearing below 0.1 V in the discharge and charge curves. Additional lithium could also be inserted through a short circuit of the cells, which allowed to demonstrate that lithium inserted at low potential is responsible for the polarization observed in the potential range from 0.1 to 1.2 V. The lithiated sample from carbon prepared with stretching exhibits a ^{7}Li NMR peak centered at 66 ppm (vs LiCl) at room temperature, which splits in two different components at low temperature: a paramagnetic contribution, which shifts to 220 ppm, and a peak independent of temperature located at 18 ppm. These results suggest that there are two different lithium species in the hard carbon: a likely covalent lithium located in graphitic type intervals responsible for the shift at 18 ppm, and a pseudo-metallic lithium forming clusters into nano-cavities and giving rise to the shift at 220 ppm at low temperature. As stated by Tatsumi et al.,[19] and recently by Guérin et al.,[24] the room-temperature spectrum is then explained by the exchange between these two main Li natures. Taking into account the increase of ^{7}Li NMR shift with increasing state-of-discharge, covalent lithium initially forms followed by the pseudo-metallic lithium. Surprisingly, both types of Li seem to be extracted after one complete cycle, a contribution at 0 ppm being only observed when the potential of the cell reaches 3 V. The polarization (so-called hysteresis) in the second part of oxidation is attributed to the extraction of pseudo-metallic lithium clusters which partially transfer charge to carbon, that requires a higher value of potential for a full back-donation of their electrons. However a ^{7}Li NMR shift of 0 ppm is not an absolute proof for the complete elimination of inserted lithium. The charge transfer on carbon should also be controlled carefully.

References and Notes

(1) Dahn, J. R.; Sleigh, A. K.; Shi, H.; Way, B. M.; Weydanz, W. J.; Reimers, J. N.; Zhong, Q.; von Sacken, U. *Lithium Batteries, New Materials, Developments and Perspectives*; Pistoia, G., Ed.; Elsevier: Amsterdam, 1994; pp 1−47.

(2) Fong, R.; von Sacken, U.; Dahn, J. R. *J. Electrochem. Soc.* **1990**, *137*, 2009.

(3) Iijima, T.; Suzuki, K.; Matsuda, Y. *Synth. Metals* **1995**, *73*, 9.

(4) Mabuchi, A.; Tokumitsu, K.; Fujimoto, H.; Kasuh, T. *J. Electrochem. Soc.* **1995**, *142*, 1041.

(5) Béguin, F. Le Carbone dans tous ses Etats; Bernier, P., Ed.; Gordon and Breach: Amsterdam, 1997; pp 405−455.

(6) Xing, W.; Xue, J. S.; Dahn, J. R. *J. Electrochem. Soc.* **1996**, *143*, 3046.

(7) Rouzaud, J. N.; Oberlin, A. *Carbon* **1989**, *27*, 517.

(8) Oberlin, A. *Chemistry and Physics of Carbon*; Thrower, P. A., Ed.; 1989; Vol. 22, pp 1−143.

(9) Sato, K.; Noguchi, M.; Demachi, A.; Oki, N.; Endo, M. *Science* **1994**, *264*, 556.

(10) Tokumitsu, K.; Mabuchi, A.; Fujimoto, H.; Kasuh, T. *J. Electrochem. Soc.* **1996**, *143*, 2235.

(11) Zheng, T.; Zhong, Q.; Dahn, J. R. *J. Electrochem. Soc*. **1995**, *142*, L211.

(12) Zheng, T.; McKinnon, W. R.; Dahn, J. R. *J. Electrochem. Soc*. **1996**, *143*, 2137.

(13) Liu, Y.; Xue, J. S.; Zheng, T.; Dahn, J. R. *Carbon* **1996**, *34*, 193.

(14) Jung, Y.; Suh, M. C.; Shim, S. C.; Kwak, J. *J. Electrochem. Soc.* **1998**, *145*, 3123.

(15) Conard, J.; Estrade, H. *Mater. Sci. Eng.* **1977**, *31*, 173.

(16) Tatsumi, K.; Kawamura, T.; Higuchi, S.; Hosotubo, T.; Nakajima, H.; Sawada, Y. *J. Power Sources* **1997**, *68*, 263.

(17) Tatsumi, K.; Conard, J.; Lauginie, P.; Menu, S. *Extended Abstracts, International Symposium on Carbon, Science and Technology for New Carbon*, Tokyo, Tanso, 1998.

(18) Imanishi, N.; Kumai, K.; Kokugan, H.; Takeda, Y.; Yamamoto, O. *Solid State Ionics* **1998**, *107*, 135.

(19) Tatsumi, K.; Conard, J.; Nakahara, M.; Menu, S.; Lauginie, P.; Sawada, Y.; Ogumi, Z. *Chem. Commun.* **1997**, 687.

(20) Dai, Y.; Wang, Y.; Eshkenaki, V.; Peled, E.; Greenbaum, G. *J. Electrochem. Soc.* **1998**, *145*, 1179.

(21) Wang, S.; Matsui, H.; Tamamura, H.; Matsumura, Y.; Yamabe, Y. *Phys. Rev. B.* **1998**, *58*, 8163.

(22) Yamazaki, S.; Hashimoto, T.; Iriyama, T.; Mori, Y.; Shiroki, H.; Tamura, N. *J. Mol. Struct.* **1998**, *441*, 165.

(23) Tatsumi, K.; Conard, J.; Nakahara, M.; Menu, S.; Lauginie, P.; Sawada, Y.; Ogumi, Z. *J. Power Sources* **1999**, *81−82*, 397.

(24) Guérin, K.; Ménétrier, M.; Février-Bouvier, A.; Flandrois, S.; Simon, B.; Biensan P. *Solid State Ionics* **2000**, *127*, 187.

(25) Conard, J.; Lauginie, P. *Tanso* **2000**, *191*, 62.

(26) Ryter, Ch. *Phys. Rev. Lett*. **1960**, *5*, 10.